

NUMERICAL ANALYSIS AND SCIENTIFIC COMPUTING
PREPRINT SERIA

**Optimization-based decoupling
algorithms for a fluid-poroelastic system**

A. CESMELIOGLU H. LEE A. QUAINI K. WANG
S.-Y. YI

PREPRINT #43



DEPARTMENT OF MATHEMATICS
UNIVERSITY OF HOUSTON

NOVEMBER 2015

Optimization-based decoupling algorithms for a fluid-poroelastic system

Aycil Cesmelioglu, Hyesuk Lee, Annalisa Quaini, Kening Wang and Son-Young Yi

Abstract In this paper, computational algorithms for the Stokes-Biot coupled system are proposed to study the interaction of a free fluid with a poroelastic material. The decoupling strategy we employ is to cast the coupled fluid-poroelastic system as a constrained optimization problem with a Neumann type control that enforces continuity of the normal components of the stress on the interface. The optimization objective is to minimize any violation of the other interface conditions. Two numerical algorithms based on a residual updating technique are presented. One solves a least squares problem and the other solves a linear problem when the fluid velocity in the poroelastic structure is smooth enough. Both algorithms yield the minimizer of the constrained optimization problem. Some numerical results are provided to validate the accuracy and efficiency of the proposed algorithms .

Aycil Cesmelioglu
Department of Mathematics and Statistics, Oakland University, Rochester, MI 48083, e-mail: cesmelio@oakland.edu

Hyesuk Lee
Department of Mathematical Sciences, Clemson University, Clemson, SC 29634 e-mail: hk-lee@clemson.edu

Annalisa Quaini
Department of Mathematics, University of Houston, Houston, TX 77204 e-mail: quaini@math.uh.edu

Kening Wang
Department of Mathematics and Statistics, University of North Florida, Jacksonville, FL 32224 e-mail: kening.wang@unf.edu

Son-Young Yi
Department of Mathematical Sciences, The University of Texas at El Paso, El Paso, TX 79968 e-mail: syi@utep.edu

1 Introduction

We develop a robust and efficient numerical method to simulate the interaction of a free fluid with a deformable porous medium. Modeling fluid-poroelastic structure interaction is of great importance in a wide range of industrial and environmental applications, including groundwater flow, oil and gas production, blood-vessel interactions, breakwater design, and many more. See, e.g., [1, 2, 3, 4, 5, 6, 7, 8, 9] and references therein.

To model the free fluid, we consider the Stokes equations for a single phase, incompressible viscous fluid. A well accepted model for the fluid flow in a deformable porous medium is the Biot system [10, 11, 12, 13]. The stress and flow couplings on the interface between the Biot flow through the deforming porous medium and the Stokes flow in the open channel must be prescribed by physically-consistent interface conditions. Refer to [14] for the formulation of the interface conditions and analytical study of the model.

The numerical discretization of the Stokes-Biot system poses great computational challenges due to the nature of its complexity. A fully-coupled scheme, which solves the Stokes and Biot subproblems simultaneously, results in a large linear system, which in turn requires a large amount of memory space and a special solver. The objective of this work is to develop efficient decoupling schemes that allow us to independently solve each subproblem using existing Stokes and Biot solvers possibly with slight modification, while ensuring convergence to an accurate solution. Recently, Bukač *et al.* [9] proposed and analyzed a loosely coupled scheme for the Stokes-Biot system, for which interface conditions are imposed for local problems by time lagging. In this work, we consider a different approach for decoupling, where the solution algorithm considered is based on optimization. We present a Neumann type control that enforces continuity of the normal components of the stress on the interface while minimizing any violation of the remaining interface conditions. Two numerical algorithms based on a residual updating technique are presented. One redefines the constrained optimization problem as a least squares problem whose solution yields the minimizer of the original constrained optimization problem. The other algorithm seeks the minimizer by solving a linear problem, assuming the fluid velocity in the poroelastic structure is smooth enough. Some numerical results are provided to validate the accuracy and efficiency of the proposed methods.

This paper is organized as follows. In Section 2 we present the governing equations of the Stokes-Biot problem, complemented by initial, boundary, and interface conditions. Time discretized weak formulation and its appropriate functional spaces are introduced in Section 3. Section 4 is devoted to the development of optimization-based decoupling schemes. Finally, in Section 5, we present some results of our numerical experiments.

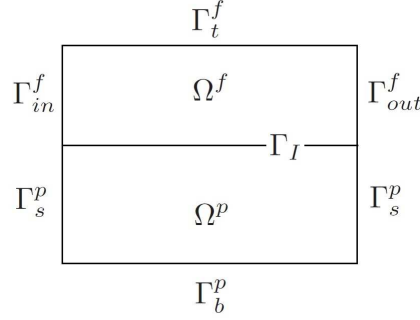


Fig. 1 Fluid-poroelastic domain

2 Model equations

Suppose that the domain under consideration is made up of two regions $\Omega^f(t) \in \mathbb{R}^2$ and $\Omega^p(t) \in \mathbb{R}^2$, t being time, separated by a common moving interface $\Gamma_{I(t)} = \partial\Omega^f(t) \cap \partial\Omega^p(t)$. See Figure 1. The first region $\Omega^f(t)$ is occupied by the free fluid and has boundary Γ^f such that $\Gamma^f = \Gamma_{in}^f \cup \Gamma_{out}^f \cup \Gamma_t^f \cup \Gamma_{I(t)}$, where Γ_{in}^f and Γ_{out}^f represent the inlet and outlet boundary, respectively. The second region $\Omega^p(t)$ is occupied by a saturated poroelastic structure with the boundary Γ^p such that $\Gamma^p = \Gamma_s^p \cup \Gamma_b^p \cup \Gamma_{I(t)}$, where $\Gamma_s^p \cup \Gamma_b^p$ represents the outer structure boundary.

For the sake of simplicity, we will consider the problem under the assumption of fixed domains $\Omega^f(t)$ and $\Omega^p(t)$. That is,

$$\Omega^f(t) = \Omega^f, \quad \Omega^p(t) = \Omega^p, \quad \Gamma_{I(t)} = \Gamma_I, \quad \forall t \in [0, T].$$

This assumption allows for a simple presentation of the algorithms to be proposed in the subsequent sections. In order to incorporate the full effect of the moving interface, we can employ the Arbitrary Lagrangian-Eulerian (ALE) formulation. Refer to [17] for a similar decoupling algorithm for fluid-structure interaction based on the ALE formulation.

Consider the fluid equations:

$$\rho_f \frac{\partial \mathbf{u}_f}{\partial t} - 2\nu_f \nabla \cdot D(\mathbf{u}_f) + \nabla p_f = \mathbf{f}_f \quad \text{in } \Omega^f, \quad (1a)$$

$$\nabla \cdot \mathbf{u}_f = 0 \quad \text{in } \Omega^f, \quad (1b)$$

where \mathbf{u}_f denotes the velocity vector of the fluid, p_f the pressure of the fluid, ρ_f the density of the fluid, ν_f the fluid viscosity, and \mathbf{f}_f the body force acting on the fluid. Here, $D(\mathbf{u}_f)$ is the strain rate tensor:

$$D(\mathbf{u}_f) = \frac{1}{2} (\nabla \mathbf{u}_f + (\nabla \mathbf{u}_f)^T).$$

The Cauchy stress tensor is given by:

$$\boldsymbol{\sigma}_f = 2\nu_f D(\mathbf{u}_f) - p_f \mathbf{I}.$$

Equation (1a) represents the conservation of linear momentum, while equation (1b) represents the conservation of mass. The poroelastic system is represented by the Biot model:

$$\rho_s \frac{\partial^2 \boldsymbol{\eta}}{\partial t^2} - 2\nu_s \nabla \cdot D(\boldsymbol{\eta}) - \lambda \nabla (\nabla \cdot \boldsymbol{\eta}) + \alpha \nabla p_p = \mathbf{f}_s \quad \text{in } \Omega^p, \quad (2a)$$

$$\kappa^{-1} \mathbf{u}_p + \nabla p_p = 0 \quad \text{in } \Omega^p, \quad (2b)$$

$$\frac{\partial}{\partial t} (s_0 p_p + \alpha \nabla \cdot \boldsymbol{\eta}) + \nabla \cdot \mathbf{u}_p = f_p \quad \text{in } \Omega^p, \quad (2c)$$

where $\boldsymbol{\eta}$ is the displacement of the structure, p_p is the pore pressure of the fluid, and \mathbf{u}_p is the fluid velocity. Here, f_p is the source/sink term and \mathbf{f}_s is the body force. The total stress tensor for the poroelastic structure is given by:

$$\boldsymbol{\sigma}_p = 2\nu_s D(\boldsymbol{\eta}) + \lambda (\nabla \cdot \boldsymbol{\eta}) \mathbf{I} - \alpha p_p \mathbf{I},$$

where ν_s and λ denote the Lamé constants for the skeleton. The density of saturated medium is denoted by ρ_s , and the hydraulic conductivity is denoted by κ . In general, κ is a symmetric positive definite tensor, but in this work we assume an isotropic porous material so that κ is a scalar quantity. The constrained specific storage coefficient is denoted by s_0 and the Biot-Willis constant by α , which is usually close to unity. In the subsequent discussion, all the physical parameters are assumed to be constant in space and time. Note that the Biot system consists of the momentum equation for the balance of total forces (2a) and the mass conservation equation (2c), along with the standard assumption of Darcy's law (2b) for the flux.

We remark that model (2) is the same used in, e.g., [9], but it is different from the model used in other references, such as [3, 5]. References [3, 5] focus on blood-vessel interaction and assume the artery wall is a saturated poroelastic medium. Since here the focus is more general, we preferred to use model (2).

In order to complete the Stokes-Biot model, (1)–(2), we provide the following boundary, initial and interface conditions :

- Boundary conditions:

$$\boldsymbol{\sigma}_f \mathbf{n}_f = -P_{in}(t) \quad \text{on } \Gamma_{in}^f, \quad (3a)$$

$$\boldsymbol{\sigma}_f \mathbf{n}_f = \mathbf{0} \quad \text{on } \Gamma_{out}^f, \quad (3b)$$

$$\mathbf{u}_f = \mathbf{0} \quad \text{on } \Gamma_t^f, \quad (3c)$$

$$\mathbf{u}_p \cdot \mathbf{n}_p = 0, \quad \eta = \mathbf{0} \quad \text{on } \Gamma_s^p, \quad (3d)$$

$$\mathbf{u}_p \cdot \mathbf{n}_p = 0, \quad \boldsymbol{\sigma}_p \mathbf{n}_p = \mathbf{0} \quad \text{on } \Gamma_b^p. \quad (3e)$$

- Initial conditions:

$$\text{At } t = 0: \quad \mathbf{u}_f = \mathbf{0}, \quad p_p = 0, \quad \eta = \mathbf{0}, \quad \eta_t = \mathbf{0}. \quad (4)$$

- Interface conditions on Γ_I :

$$\mathbf{u}_f \cdot \mathbf{n}_f = -(\eta_t + \mathbf{u}_p) \cdot \mathbf{n}_p, \quad (5a)$$

$$\boldsymbol{\sigma}_f \mathbf{n}_f = -\boldsymbol{\sigma}_p \mathbf{n}_p, \quad (5b)$$

$$\mathbf{n}_f \cdot \boldsymbol{\sigma}_f \mathbf{n}_f = -p_p, \quad (5c)$$

$$\mathbf{n}_f \cdot \boldsymbol{\sigma}_f \mathbf{t} = -\beta(\mathbf{u}_f - \eta_t) \cdot \mathbf{t}, \quad (5d)$$

where \mathbf{n}_f and \mathbf{n}_p denote outward unit normal vectors to Ω^f and Ω^p , respectively, \mathbf{t} denotes a unit tangent vector on Γ_I , and β denotes the resistance parameter in the tangential direction.

Here, (5a) describes the admissibility constraint. The conservation of momentum, expressed by (5b), requires that the total stress of the porous medium be balanced by the total stress of the fluid. For the balance of normal components of the stress in the fluid phase across the interface, we have (5c). Finally, the tangential stress of the fluid is assumed to be proportional to the slip rate according to the Beavers-Joseph-Saffman condition (5d). These interface conditions suffice to precisely couple the Stokes system (1) to the Biot system (2).

3 Semi-discrete weak formulation

Standard notation for Sobolev spaces and their associated norms and seminorms will be used to define a weak formulation of the problem. For example, $W^{m,p}(\Theta)$ is the usual Sobolev space with the norm $\|\cdot\|_{m,p,\Theta}$. In case of $p = 2$, the Sobolev space $W^{m,2}(\Theta)$ is denoted by $H^m(\Theta)$ with the norm $\|\cdot\|_{m,\Theta}$. When $m = 0$, $H^m(\Theta)$ coincides with $L^2(\Theta)$. In this case, the inner product and the norm will be denoted by $(\cdot, \cdot)_\Theta$ and $\|\cdot\|_\Theta$, respectively. Moreover, if $\Theta = \Omega^f$ or Ω^p , and the context is clear, Θ will be omitted, i.e., $(\cdot, \cdot) = (\cdot, \cdot)_{\Omega^f}$ or $(\cdot, \cdot)_{\Omega^p}$ for functions defined in Ω^f and Ω^p . For $\gamma \subset \partial\Omega^f \cup \partial\Omega^p$, we use $\langle \cdot, \cdot \rangle_\gamma$ to denote the duality pairing between

$H^{-1/2}(\gamma)$ and $H^{1/2}(\gamma)$. Finally, the associated space of vector valued functions will be denoted by a boldface font.

Now, we are in a position to define the following function spaces for the velocities $\mathbf{u}_f, \mathbf{u}_p$, the pressures p_f, p_p , and the displacement η , respectively:

$$\begin{aligned} \mathbf{U}_f &:= \{\mathbf{v} \in \mathbf{H}^1(\Omega^f) : \mathbf{v} = \mathbf{0} \text{ on } \Gamma_t^f\}, \\ \mathbf{U}_p &:= \mathbf{H}_{0, \Gamma_s^p \cup \Gamma_b^p}^{div}(\Omega^p) = \{\mathbf{v} \in \mathbf{L}^2(\Omega^p) : \nabla \cdot \mathbf{v} \in L^2(\Omega^p), \mathbf{v} \cdot \mathbf{n}_p = 0 \text{ on } \Gamma_s^p \cup \Gamma_b^p\}, \\ Q_f &:= L^2(\Omega^f), \\ Q_p &:= L^2(\Omega^p), \\ \Sigma &:= \{\xi \in \mathbf{H}^1(\Omega^p) : \xi = \mathbf{0} \text{ on } \Gamma_s^p\}. \end{aligned}$$

We also define

$$\mathbf{G} := \mathbf{H}^{1/2}(\Gamma_I)$$

for the space of the control function to be introduced later.

Multiplying the governing equations (1) and (2) by appropriate test functions and using integration by parts, we obtain a continuous variational formulation for the fluid problem:

$$\begin{aligned} \rho_f \left(\frac{\partial \mathbf{u}_f}{\partial t}, \mathbf{v}_f \right) + 2\nu_f (D(\mathbf{u}_f), D(\mathbf{v}_f)) - (p_f, \nabla \cdot \mathbf{v}_f) \\ = (\mathbf{f}_f, \mathbf{v}_f) + \langle -P_m, \mathbf{v}_f \rangle_{\Gamma_m^f} + \langle \sigma_f \mathbf{n}_f, \mathbf{v}_f \rangle_{\Gamma_I}, \quad \forall \mathbf{v}_f \in \mathbf{U}_f, \end{aligned} \quad (1a)$$

$$(q_f, \nabla \cdot \mathbf{u}_f) = 0, \quad \forall q_f \in Q_f, \quad (1b)$$

and for the structure problem:

$$\begin{aligned} \rho_s \left(\frac{\partial^2 \eta}{\partial t^2}, \xi \right) + 2\nu_s (D(\eta), D(\xi)) + \lambda (\nabla \cdot \eta, \nabla \cdot \xi) - \alpha (p_p, \nabla \cdot \xi) \\ = (\mathbf{f}_s, \xi) + \langle \sigma_p \mathbf{n}_p, \xi \rangle_{\Gamma_I}, \quad \forall \xi \in \Sigma, \end{aligned} \quad (2a)$$

$$\kappa^{-1} (\mathbf{u}_p, \mathbf{v}_p) - (p_p, \nabla \cdot \mathbf{v}_p) = \langle -p_p, \mathbf{v}_p \cdot \mathbf{n}_p \rangle_{\Gamma_I}, \quad \forall \mathbf{v}_p \in \mathbf{U}_p, \quad (2b)$$

$$\left(q_p, \frac{\partial}{\partial t} (s_0 p_p + \alpha \nabla \cdot \eta) + \nabla \cdot \mathbf{u}_p \right) = (q_p, f_p), \quad \forall q_p \in Q_p. \quad (2c)$$

Before we discretize the above equations in time, we introduce some notation first. Let $\Delta t = T/N$, where N is a positive integer and let $t^n = n\Delta t$. For any sufficiently smooth function $v(t, \mathbf{x})$, both constant and vector-valued, we define $v^n(\mathbf{x}) = v(t^n, \mathbf{x})$.

For the time discretization of the Stokes problem (1), we use the Backward Euler scheme. Then, the discrete-in-time, continuous-in-space problem of the free fluid reads as follows: For $n = 1, 2, \dots, N$, find $\mathbf{u}_f^n \in \mathbf{U}_f$ and $p_f^n \in Q_f$ such that

$$\begin{aligned} \rho_f \left(\frac{\mathbf{u}_f^n - \mathbf{u}_f^{n-1}}{\Delta t}, \mathbf{v}_f \right) + 2\nu_f(D(\mathbf{u}_f^n), D(\mathbf{v}_f)) - (p_f^n, \nabla \cdot \mathbf{v}_f) \\ = (\mathbf{f}_f^n, \mathbf{v}_f) + \langle -P_{in}^n, \mathbf{v}_f \rangle_{\Gamma_m^f} + \langle \sigma_f^n \mathbf{n}_f, \mathbf{v}_f \rangle_{\Gamma}, \quad \forall \mathbf{v}_f \in \mathbf{U}_f, \end{aligned} \quad (3a)$$

$$(q_f, \nabla \cdot \mathbf{u}_f^n) = 0, \quad \forall q_f \in Q_f. \quad (3b)$$

On the other hand, the semi-discrete problem of the Biot model is: For $n = 1, 2, \dots, N$, find $\eta^n \in \Sigma$, $\mathbf{u}_p^n \in \mathbf{U}_p$, and $p_p^n \in Q_p$ such that

$$\begin{aligned} \rho_s \left(\frac{\eta^n - 2\eta^{n-1} + \eta^{n-2}}{\Delta t^2}, \xi \right) + 2\nu_s(D(\eta^n), D(\xi)) + \lambda(\nabla \cdot \eta^n, \nabla \cdot \xi) \\ - \alpha(p_p^n, \nabla \cdot \xi) = (\mathbf{f}_s^n, \xi) + \langle \sigma_p^n \mathbf{n}_p, \xi \rangle_{\Gamma}, \quad \forall \xi \in \Sigma, \end{aligned} \quad (4a)$$

$$\kappa^{-1}(\mathbf{u}_p^n, \mathbf{v}_p) - (p_p^n, \nabla \cdot \mathbf{v}_p) = \langle -p_p^n, \mathbf{v}_p \cdot \mathbf{n}_p \rangle_{\Gamma}, \quad \forall \mathbf{v}_p \in \mathbf{U}_p, \quad (4b)$$

$$\left(q_p, s_0 \frac{p_p^n - p_p^{n-1}}{\Delta t} + \alpha \frac{\nabla \cdot \eta^n - \nabla \cdot \eta^{n-1}}{\Delta t} + \nabla \cdot \mathbf{u}_p^n \right) = (q_p, f_p^n), \quad \forall q_p \in Q_p. \quad (4c)$$

The fully-coupled scheme simultaneously solves these two subproblems, (3) and (4), coupled through the interface conditions (5).

4 Decoupling schemes

The goal of this section is to develop efficient decoupling schemes that allow us to independently solve each subproblem while ensuring convergence to an accurate solution.

Let $\mathbf{g}^n = (g_1^n, g_2^n)^T := (\sigma_f^n \mathbf{n}_f)|_{\Gamma}$. Then, using the interface condition (5b), we can rewrite (3a) and (4a), respectively, as

$$\begin{aligned} \rho_f \left(\frac{\mathbf{u}_f^n - \mathbf{u}_f^{n-1}}{\Delta t}, \mathbf{v}_f \right) + 2\nu_f(D(\mathbf{u}_f^n), D(\mathbf{v}_f)) - (p_f^n, \nabla \cdot \mathbf{v}_f) \\ = (\mathbf{f}_f^n, \mathbf{v}_f) + \langle -P_{in}^n, \mathbf{v}_f \rangle_{\Gamma_m^f} + \langle \mathbf{g}^n, \mathbf{v}_f \rangle_{\Gamma}, \quad \forall \mathbf{v}_f \in \mathbf{U}_f, \\ \rho_s \left(\frac{\eta^n - 2\eta^{n-1} + \eta^{n-2}}{\Delta t^2}, \xi \right) + 2\nu_s(D(\eta^n), D(\xi)) + \lambda(\nabla \cdot \eta^n, \nabla \cdot \xi) \\ - \alpha(p_p^n, \nabla \cdot \xi) = (\mathbf{f}_s^n, \xi) - \langle \mathbf{g}^n, \xi \rangle_{\Gamma}. \quad \forall \xi \in \Sigma. \end{aligned}$$

On the other hand, we can rewrite

$$\mathbf{g}^n = ((\mathbf{n}_f \cdot \sigma_f^n \mathbf{n}_f) \mathbf{n}_f + (\mathbf{t} \cdot \sigma_f^n \mathbf{n}_f) \mathbf{t})|_{\Gamma}, \quad (1)$$

which, together with (5c), implies that

$$-p_p|_{\Gamma} = (\mathbf{n}_f \cdot \boldsymbol{\sigma}_f^n \mathbf{n}_f)|_{\Gamma} = \mathbf{g}^n \cdot \mathbf{n}_f = -\mathbf{g}^n \cdot \mathbf{n}_p.$$

Then, (4b) can be rewritten as

$$\kappa^{-1}(\mathbf{u}_p^n, \mathbf{v}_p) - (p_p^n, \nabla \cdot \mathbf{v}_p) = -\langle \mathbf{g}^n \cdot \mathbf{n}_p, \mathbf{v}_p \cdot \mathbf{n}_p \rangle_{\Gamma}, \quad \forall \mathbf{v}_p \in \mathbf{U}_p.$$

In summary, the semi-discrete Stokes and Biot problems, (3) and (4), can be rewritten in terms of \mathbf{g}^n :

$$\begin{aligned} \rho_f \left(\frac{\mathbf{u}_f^n - \mathbf{u}_f^{n-1}}{\Delta t}, \mathbf{v}_f \right) + 2\nu_f(D(\mathbf{u}_f^n), D(\mathbf{v}_f)) - (p_f^n, \nabla \cdot \mathbf{v}_f) \\ = (\mathbf{f}_f^n, \mathbf{v}_f) + \langle -P_{in}, \mathbf{v}_f \rangle_{\Gamma_{in}^f} + \langle \mathbf{g}^n, \mathbf{v}_f \rangle_{\Gamma}, \quad \forall \mathbf{v}_f \in \mathbf{U}_f, \end{aligned} \quad (2a)$$

$$(q_f, \nabla \cdot \mathbf{u}_f^n) = 0, \quad \forall q_f \in Q_f. \quad (2b)$$

and

$$\begin{aligned} \rho_s \left(\frac{\eta^n - 2\eta^{n-1} + \eta^{n-2}}{\Delta t^2}, \xi \right) + 2\nu_s(D(\eta^n), D(\xi)) + \lambda(\nabla \cdot \eta^n, \nabla \cdot \xi) \\ - \alpha(p_p^n, \nabla \cdot \xi) = (\mathbf{f}_s^n, \xi) - \langle \mathbf{g}^n, \xi \rangle_{\Gamma}, \quad \forall \xi \in \Sigma, \end{aligned} \quad (3a)$$

$$\kappa^{-1}(\mathbf{u}_p^n, \mathbf{v}_p) - (p_p^n, \nabla \cdot \mathbf{v}_p) = -\langle \mathbf{g}^n \cdot \mathbf{n}_p, \mathbf{v}_p \cdot \mathbf{n}_p \rangle_{\Gamma}, \quad \forall \mathbf{v}_p \in \mathbf{U}_p, \quad (3b)$$

$$\left(q_p, s_0 \frac{p_p^n - p_p^{n-1}}{\Delta t} + \alpha \frac{\nabla \cdot \eta^n - \nabla \cdot \eta^{n-1}}{\Delta t} + \nabla \cdot \mathbf{u}_p^n \right) = (q_p, f_p^n), \quad \forall q_p \in Q_p. \quad (3c)$$

Note that these two subproblems are coupled through the function \mathbf{g}^n only. If \mathbf{g}^n is known at each time step n , then the two subproblems can be completely decoupled. However, \mathbf{g}^n is unknown as $\boldsymbol{\sigma}_f^n$ is unknown.

Here, we will cast this fully-coupled problem as a constrained optimization problem using \mathbf{g}^n as our control function. With an arbitrarily chosen \mathbf{g}^n , the solutions of (2) and (3) are not the same solutions for (3) and (4). It is because two interface conditions (5b) and (5c) are incorporated in the formulation, but the remaining interface conditions, (5a) and (5d) are not. Therefore, the objective of our optimization is to minimize the violation of (5a) and (5d). In order to do that, let the interface boundary Γ be partitioned into non-overlapping segments Γ_i for $i = 1, 2, \dots, k$ such that $\Gamma = \cup_{i=1}^k \Gamma_i$. To satisfy the interface condition (5a) and (5d) at each time step n , we want to find a function $\mathbf{g}^n \in \mathbf{G}$ such that (\mathbf{u}_f^n, p_f^n) satisfying (2) and $(\mathbf{u}_p^n, p_p^n, \eta^n)$ satisfying (3) minimize the functional

$$\begin{aligned} \mathcal{J}_n(\mathbf{g}^n) := & \frac{1}{2} \sum_{i=1}^k \left(\frac{1}{\sqrt{|\Gamma_i|}} \int_{\Gamma_i} \mathbf{u}_f^n \cdot \mathbf{n}_f + \left(\frac{\eta^n - \eta^{n-1}}{\Delta t} + \mathbf{u}_p^n \right) \cdot \mathbf{n}_p \, d\Gamma_i \right)^2 \\ & + \frac{1}{2} \left\| \mathbf{g}^n \cdot \mathbf{t} + \left(\beta \left(\mathbf{u}_f^n - \frac{\eta^n - \eta^{n-1}}{\Delta t} \right) \cdot \mathbf{t} \right) \Big|_{\Gamma_i} \right\|_{0, \Gamma_i}^2 + \frac{1}{2} \delta \|\mathbf{g}^n\|_{\mathbf{G}}^2, \end{aligned} \quad (4)$$

where $|\gamma| := \text{meas}(\gamma)$ for $\gamma \subset \partial\Omega_f \cup \partial\Omega_p$ and $\delta > 0$ is a penalty parameter.

Minimizing the first term of the function in (4) seeks to weakly impose (5a) by forcing *flow balance* across the interface segments Γ_i . See [15] for details. The minimization of the second term in (4) is for the weak imposition of the Beavers-Joseph-Saffman condition (5d). Finally, the last term in (4) is a penalty term.

Remark 1. Thanks to (1), we can write $\mathbf{g}^n \cdot \mathbf{t}$ in place of $(\mathbf{n}_f \cdot \boldsymbol{\sigma}_f^n)|_{\Gamma_i}$ in $\mathcal{J}_n(\mathbf{g}^n)$.

4.1 Least squares method

In this section, we are going to redefine the minimization problem as a least squares problem.

Set $\mathbf{F} = \mathbb{R}^k \times L^2(\Gamma) \times \mathbf{G}$ and define the operator $N_n : \mathbf{G} \rightarrow \mathbf{F}$ as

$$N_n(\mathbf{g}^n) = \begin{pmatrix} \frac{1}{\sqrt{|\Gamma_1|}} \int_{\Gamma_1} \mathbf{u}_f^n \cdot \mathbf{n}_f + \left(\frac{\eta^n - \eta^{n-1}}{\Delta t} + \mathbf{u}_p^n \right) \cdot \mathbf{n}_p \, d\Gamma_1 \\ \vdots \\ \frac{1}{\sqrt{|\Gamma_k|}} \int_{\Gamma_k} \mathbf{u}_f^n \cdot \mathbf{n}_f + \left(\frac{\eta^n - \eta^{n-1}}{\Delta t} + \mathbf{u}_p^n \right) \cdot \mathbf{n}_p \, d\Gamma_k \\ \mathbf{g}^n \cdot \mathbf{t} + \left(\beta \left(\mathbf{u}_f^n - \frac{\eta^n - \eta^{n-1}}{\Delta t} \right) \cdot \mathbf{t} \right) \Big|_{\Gamma} \\ \sqrt{\delta} \mathbf{g}^n \end{pmatrix}, \quad (5)$$

where $(\mathbf{u}_f^n, \mathbf{u}_p^n)$ is the solution of (2) and $(\mathbf{u}_p^n, p_p^n, \eta^n)$ is the solution of (3).

The minimization of the functional $\mathcal{J}_n(\mathbf{g}^n)$ in (4) is then equivalent to the minimization of the least squares function $\|N_n(\mathbf{g}^n)\|_{\mathbf{F}}^2$, that is:

$$\min_{\mathbf{g}^n \in \mathbf{G}} \mathcal{J}_n(\mathbf{g}^n) = \frac{1}{2} \min_{\mathbf{g}^n \in \mathbf{G}} \|N_n(\mathbf{g}^n)\|_{\mathbf{F}}^2. \quad (6)$$

We solve this problem by a residual updating technique. First, an initial guess for a minimizer, $\mathbf{g}_{(0)}^n$, is chosen and $N_n(\mathbf{g}_{(0)}^n)$ is computed. Since we expect that $N_n(\mathbf{g}^n) \approx [\mathbf{0} \sqrt{\delta} \mathbf{g}^n]^T$ for a sufficiently small δ at the minimizer, we take $N_n(\mathbf{g}_{(0)}^n) - [\mathbf{0} \sqrt{\delta} \mathbf{g}_{(0)}^n]^T$ as a residual and find a correction \mathbf{h}^n for $\mathbf{g}_{(0)}^n$ such that

$$\begin{aligned} & \frac{1}{2} \left\| \left(N_n(\mathbf{g}_{(0)}^n) - [\mathbf{0} \sqrt{\delta} \mathbf{g}_{(0)}^n]^T \right) + N'_n(\mathbf{g}_{(0)}^n)(\mathbf{h}^n) \right\|_{\mathbf{F}}^2 \\ &= \min_{\mathbf{y} \in \mathbf{G}} \frac{1}{2} \left\| \left(N_n(\mathbf{g}_{(0)}^n) - [\mathbf{0} \sqrt{\delta} \mathbf{g}_{(0)}^n]^T \right) + N'_n(\mathbf{g}_{(0)}^n)(\mathbf{y}) \right\|_{\mathbf{F}}^2. \end{aligned} \quad (7)$$

Here, $N'_n(\mathbf{g}_{(0)}^n)(\cdot) : \mathbf{G} \rightarrow \mathbf{F}$ is defined by

$$N'_n(\mathbf{g}_{(0)}^n)(\mathbf{h}^n) = \begin{pmatrix} \frac{1}{\sqrt{|\Gamma_1|}} \int_{\Gamma_1} \mathbf{w}_f^n \cdot \mathbf{n}_f + \left(\frac{\varphi^n}{\Delta t} + \mathbf{w}_p^n \right) \cdot \mathbf{n}_p \, d\Gamma_1 \\ \vdots \\ \frac{1}{\sqrt{|\Gamma_k|}} \int_{\Gamma_k} \mathbf{w}_f^n \cdot \mathbf{n}_f + \left(\frac{\varphi^n}{\Delta t} + \mathbf{w}_p^n \right) \cdot \mathbf{n}_p \, d\Gamma_k \\ \mathbf{h}^n \cdot \mathbf{t} + \left(\beta \left(\mathbf{w}_f^n - \frac{\varphi^n}{\Delta t} \right) \cdot \mathbf{t} \right) \Big|_{\Gamma} \\ \sqrt{\delta} \mathbf{h}^n \end{pmatrix}, \quad (8)$$

where $(\mathbf{w}_f^n, \phi_f^n)$ is the solution of the problem:

$$\rho_f \left(\frac{\mathbf{w}_f^n}{\Delta t}, \mathbf{v}_f \right) + 2\nu_f (D(\mathbf{w}_f^n), D(\mathbf{v}_f)) - (\phi_f^n, \nabla \cdot \mathbf{v}_f) = \langle \mathbf{h}^n, \mathbf{v}_f \rangle_{\Gamma}, \quad \forall \mathbf{v}_f \in \mathbf{U}_f, \quad (9a)$$

$$(q_f, \nabla \cdot \mathbf{w}_f^n) = 0, \quad \forall q_f \in Q_f, \quad (9b)$$

and $(\mathbf{w}_p^n, \phi_p^n, \varphi^n)$ is the solution of the problem:

$$\begin{aligned} \rho_s \left(\frac{\varphi^n}{\Delta t^2}, \xi \right) + 2\nu_s (D(\varphi^n), D(\xi)) + \lambda (\nabla \cdot \varphi^n, \nabla \cdot \xi) \\ - \alpha (\phi_p^n, \nabla \cdot \xi) = -\langle \mathbf{h}^n, \xi \rangle_{\Gamma}, \quad \forall \xi \in \Sigma, \end{aligned} \quad (10a)$$

$$\kappa^{-1} (\mathbf{w}_p^n, \mathbf{v}_p) - (\phi_p^n, \nabla \cdot \mathbf{v}_p) = -\langle \mathbf{h}^n \cdot \mathbf{n}_p, \mathbf{v}_p \cdot \mathbf{n}_p \rangle_{\Gamma}, \quad \forall \mathbf{v}_p \in \mathbf{U}_p, \quad (10b)$$

$$\left(q_p, s_0 \frac{\phi_p^n}{\Delta t} + \alpha \frac{\nabla \cdot \varphi^n}{\Delta t} + \nabla \cdot \mathbf{w}_p^n \right) = 0, \quad \forall q_p \in Q_p. \quad (10c)$$

In order to solve the minimization problem (7), we solve its normal equation

$$N'_n(\mathbf{g}_{(0)}^n)^* N'_n(\mathbf{g}_{(0)}^n)(\mathbf{h}^n) = -N'_n(\mathbf{g}_{(0)}^n)^* \left(N_n(\mathbf{g}_{(0)}^n) - [\mathbf{0} \sqrt{\delta} \mathbf{g}_{(0)}^n]^T \right), \quad (11)$$

where $N'_n(\mathbf{g}_{(0)}^n)^* : \mathbb{R}^k \times L^2(\Gamma) \times \mathbf{G}^* \rightarrow \mathbf{G}^*$ is the adjoint operator of $N'_n(\mathbf{g}_{(0)}^n)$ identified in the following lemma.

Lemma 1. For $(\gamma, y, \mathbf{z}) \in \mathbb{R}^k \times L^2(\Gamma) \times \mathbf{G}^*$, the adjoint of $N'_n(\mathbf{g}_{(0)}^n)$ is given by

$$N'_n(\mathbf{g}_{(0)}^n)^* \begin{pmatrix} \gamma \\ y \\ \mathbf{z} \end{pmatrix} = \left(\bar{\mathbf{w}}_f^n - \bar{\varphi}^n - (\bar{\mathbf{w}}_p^n \cdot \mathbf{n}_p) \mathbf{n}_p \right) \Big|_{\Gamma} + y \mathbf{t} + \sqrt{\delta} \mathbf{z}, \quad (12)$$

where $(\bar{\mathbf{w}}_f^n, \bar{\varphi}^n)$ is the solution of

$$\begin{aligned} \rho_f \left(\frac{\bar{\mathbf{w}}_f^n}{\Delta t}, \mathbf{v}_f \right) + 2\nu_f (D(\bar{\mathbf{w}}_f^n), D(\mathbf{v}_f)) - (\bar{\phi}_f^n, \nabla \cdot \mathbf{v}_f) \\ = \beta \langle y, \mathbf{v}_f \cdot \mathbf{t} \rangle_{\Gamma} + \sum_{i=1}^k \gamma_i \frac{1}{\sqrt{|\Gamma_i|}} \int_{\Gamma_i} \mathbf{v}_f \cdot \mathbf{n}_f d\Gamma_i, \quad \forall \mathbf{v}_f \in \mathbf{U}_f, \end{aligned} \quad (13a)$$

$$(q_f, \nabla \cdot \bar{\mathbf{w}}_f^n) = 0, \quad \forall q_f \in \mathcal{Q}_f, \quad (13b)$$

and $(\bar{\mathbf{w}}_p^n, \bar{\phi}_p^n, \bar{\varphi}_p^n)$ is the solution of

$$\begin{aligned} \rho_s \left(\frac{\bar{\phi}_p^n}{\Delta t^2}, \xi \right) + 2\nu_s (D(\bar{\phi}_p^n), D(\xi)) + \lambda (\nabla \cdot \bar{\phi}_p^n, \nabla \cdot \xi) + \frac{\alpha}{\Delta t} (\bar{\phi}_p^n, \nabla \cdot \xi) \\ = -\frac{\beta}{\Delta t} \langle y, \xi \cdot \mathbf{t} \rangle_{\Gamma} + \frac{1}{\Delta t} \sum_{i=1}^k \gamma_i \frac{1}{\sqrt{|\Gamma_i|}} \int_{\Gamma_i} \xi \cdot \mathbf{n}_p d\Gamma_i, \quad \forall \xi \in \Sigma, \end{aligned} \quad (14a)$$

$$\kappa^{-1} (\bar{\mathbf{w}}_p^n, \mathbf{v}_p) + (\bar{\phi}_p^n, \nabla \cdot \mathbf{v}_p) = \sum_{i=1}^k \gamma_i \frac{1}{\sqrt{|\Gamma_i|}} \int_{\Gamma_i} \mathbf{v}_p \cdot \mathbf{n}_p d\Gamma_i, \quad \forall \mathbf{v}_p \in \mathbf{U}_p, \quad (14b)$$

$$(q_p, s_0 \frac{\bar{\phi}_p^n}{\Delta t} - \alpha \nabla \cdot \bar{\phi}_p^n - \nabla \cdot \bar{\mathbf{w}}_p^n) = 0, \quad \forall q_p \in \mathcal{Q}_p. \quad (14c)$$

Proof. Taking $(\mathbf{v}_f, q_f) = (\bar{\mathbf{w}}_f^n, \bar{\phi}_f^n)$, $(\mathbf{v}_p, q_p, \xi) = (\bar{\mathbf{w}}_p^n, \bar{\phi}_p^n, \bar{\varphi}_p^n)$ in (9) and (10), respectively, and $(\mathbf{v}_f, q_f) = (\mathbf{w}_f^n, \phi_f^n)$, $(\mathbf{v}_p, q_p, \eta) = (\mathbf{w}_p^n, \phi_p^n, \varphi_p^n)$ in (13) and (14), respectively, we obtain

$$\begin{aligned} \langle \mathbf{h}^n, \bar{\mathbf{w}}_f^n - \bar{\phi}_p^n - (\bar{\mathbf{w}}_p^n \cdot \mathbf{n}_p) \mathbf{n}_p \rangle_{\Gamma} = \sum_{i=1}^k \gamma_i \frac{1}{\sqrt{|\Gamma_i|}} \int_{\Gamma_i} \mathbf{w}_f^n \cdot \mathbf{n}_f + \left(\frac{\varphi_p^n}{\Delta t} + \mathbf{w}_p^n \right) \cdot \mathbf{n}_p d\Gamma_i \\ + \left\langle y, \beta \left(\mathbf{w}_f^n - \frac{\varphi_p^n}{\Delta t} \right) \cdot \mathbf{t} \right\rangle_{\Gamma}. \end{aligned} \quad (15)$$

Hence, by (8), (12), and (15), for $\mathbf{h}^n \in \mathbf{G}$ we have:

$$\begin{aligned} \left(N_n'(\mathbf{g}_n^0)(\mathbf{h}^n), \begin{bmatrix} \gamma \\ y \\ \mathbf{z} \end{bmatrix} \right) &= \sum_{i=1}^k \gamma_i \frac{1}{\sqrt{|\Gamma_i|}} \int_{\Gamma_i} \mathbf{w}_f^n \cdot \mathbf{n}_f + \left(\frac{\varphi_p^n}{\Delta t} + \mathbf{w}_p^n \right) \cdot \mathbf{n}_p d\Gamma_i \\ &+ \left\langle y, \mathbf{h}^n \cdot \mathbf{t} + \beta \left(\mathbf{w}_f^n - \frac{\varphi_p^n}{\Delta t} \right) \cdot \mathbf{t} \right\rangle_{\Gamma} + \sqrt{\delta} \langle \mathbf{h}^n, \mathbf{z} \rangle_{\Gamma} \\ &= \langle \mathbf{h}^n, \bar{\mathbf{w}}_f^n - \bar{\phi}_p^n - (\bar{\mathbf{w}}_p^n \cdot \mathbf{n}_p) \mathbf{n}_p + y \mathbf{t} + \sqrt{\delta} \mathbf{z} \rangle_{\Gamma} \\ &= \left(\mathbf{h}^n, N_n'(\mathbf{g}_n^0)^* \left(\begin{bmatrix} \gamma \\ y \\ \mathbf{z} \end{bmatrix} \right) \right). \end{aligned}$$

For the solution of (11), we use the Conjugate Gradient (CG) algorithm; see, e.g., [16]. The steps of the CG algorithm applied to the solution of problem $A^* A \mathbf{x} = A^* \mathbf{b}$

are described in Algorithm 1. Here, ε is a prescribed error tolerance. Note that the normal equation does not need to be formed explicitly for the algorithm.

Algorithm 1 Conjugate Gradient (CG) method for the least squares problem

1. Initialize $\mathbf{x}_{(0)}$.
 2. Set $\mathbf{r}_{(0)} = \mathbf{b} - A\mathbf{x}_{(0)}$, $\mathbf{p}_{(0)} = A^*\mathbf{r}_{(0)}$.
 3. For $i = 0, 1, 2, \dots$,
 - a. if $\|A^*\mathbf{r}_{(i)}\| < \varepsilon$, stop,
 - b. $\sigma_{(i)} = \|A^*\mathbf{r}_{(i)}\|^2 / \|A\mathbf{p}_{(i)}\|^2$,
 - c. $\mathbf{x}_{(i+1)} = \mathbf{x}_{(i)} + \sigma_{(i)}\mathbf{p}_{(i)}$,
 - d. $\mathbf{r}_{(i+1)} = \mathbf{r}_{(i)} - \sigma_{(i)}A\mathbf{p}_{(i)}$,
 - e. $\tau_{(i)} = \|A^*\mathbf{r}_{(i+1)}\|^2 / \|A^*\mathbf{r}_{(i)}\|^2$,
 - f. $\mathbf{p}_{(i+1)} = A^*\mathbf{r}_{(i+1)} + \tau_{(i)}\mathbf{p}_{(i)}$.
-

Once \mathbf{h}^n has been computed, the least squares problem (6) can be solved using the residual updating algorithm described in Algorithm 2.

Algorithm 2 Residual updating algorithm

1. Initialize $\mathbf{g}_{(0)}^n$,
 2. Solve Stokes/Biot problem defined by (2) and (3) to get $\mathbf{u}_f^n, p_f^n, \mathbf{u}_p^n, p_p^n$, and η^n ,
 3. Compute $N(\mathbf{g}_{(0)}^n)$,
 4. Find the correction \mathbf{h}^n using the CG algorithm (Algorithm 1) with $A = N'_n(\mathbf{g}_{(0)}^n)$, $\mathbf{b} = -(N_n(\mathbf{g}_{(0)}^n) - [\mathbf{0} \ \sqrt{\delta}\mathbf{g}_{(0)}^n]^T)$, $\mathbf{x} = \mathbf{h}^n$,
 5. $\mathbf{g}^n \leftarrow \mathbf{g}_{(0)}^n + \mathbf{h}^n$.
-

4.2 Linear equation

In this section, we suppose that \mathbf{u}_p^n is regular enough that $\mathbf{u}_p^n \cdot \mathbf{n}_p \in L^2(\Gamma_I)$. In this case, the objective functional \mathcal{J}_n can be defined as:

$$\begin{aligned}
\mathcal{J}_n(\mathbf{g}^n) &:= \frac{1}{2} \left\| \left(\mathbf{u}_f^n \cdot \mathbf{n}_f + \left(\frac{\eta^n - \eta^{n-1}}{\Delta t} + \mathbf{u}_p^n \right) \cdot \mathbf{n}_p \right) \Big|_{\Gamma_I} \right\|_{L^2(\Gamma_I)}^2 \\
&\quad + \frac{1}{2} \left\| \mathbf{g}^n \cdot \mathbf{t} + \beta \left(\left(\mathbf{u}_f^n - \frac{\eta^n - \eta^{n-1}}{\Delta t} \right) \cdot \mathbf{t} \right) \Big|_{\Gamma_I} \right\|_{L^2(\Gamma_I)}^2 \\
&\quad + \frac{1}{2} \delta \|\mathbf{g}^n\|_{\mathbf{G}}^2.
\end{aligned} \tag{16}$$

Assuming no penalty term in (16) and choosing a control space $\mathbf{G} := \mathbf{L}^2(\Gamma_I)$, define the linear operator $L_n : \mathbf{G} \rightarrow \mathbf{G}$ by

$$L_n(\mathbf{g}^n) = \begin{pmatrix} \left(\mathbf{u}_f^n \cdot \mathbf{n}_f + \left(\frac{\eta^n - \eta^{n-1}}{\Delta t} + \mathbf{u}_p^n \right) \cdot \mathbf{n}_p \right) \Big|_{\Gamma_I} \\ \mathbf{g}^n \cdot \mathbf{t} + \beta \left(\mathbf{u}_f^n - \frac{\eta^n - \eta^{n-1}}{\Delta t} \right) \cdot \mathbf{t} \Big|_{\Gamma_I} \end{pmatrix}, \tag{17}$$

where (\mathbf{u}_f^n, p_f^n) satisfies (2) and $(\mathbf{u}_p^n, p_p^n, \eta^n)$ satisfies (3). Assuming further that the unknown stress \mathbf{g}^n and unknowns $\mathbf{u}_f^n, \mathbf{u}_p^n, \eta^n$ have the same number of degrees of freedom on the interface when discretized (this is easily achieved by using a fluid mesh and a structure mesh that match at the interface), we can convert the minimization problem to the following linear problem:

$$\text{Find } \mathbf{g}^n \in \mathbf{G} \text{ such that } L_n(\mathbf{g}^n) = \mathbf{0}. \tag{18}$$

We can solve (18) using a residual updating technique described in Algorithm 4: For a given initial guess $\mathbf{g}_{(0)}^n$, find \mathbf{h}^n such that

$$L_n(\mathbf{g}_{(0)}^n) + L_n'(\mathbf{g}_{(0)}^n)(\mathbf{h}^n) = 0$$

and update \mathbf{g}^n . Here, $L_n' : \mathbf{G} \rightarrow \mathbf{G}$ is defined by

$$L_n'(\mathbf{g}_{(0)}^n)(\mathbf{h}^n) = \begin{pmatrix} \left(\mathbf{w}_f^n \cdot \mathbf{n}_f + \left(\frac{\phi^n}{\Delta t} + \mathbf{w}_p^n \right) \cdot \mathbf{n}_p \right) \Big|_{\Gamma_I} \\ \mathbf{h}^n \cdot \mathbf{t} + \beta \left(\mathbf{w}_f^n - \frac{\phi^n}{\Delta t} \right) \cdot \mathbf{t} \Big|_{\Gamma_I} \end{pmatrix}, \tag{19}$$

where $(\mathbf{w}_f^n, \phi_f^n)$ is the solution to (9) and $(\mathbf{w}_p^n, \phi_p^n, \phi^n)$ is the solution to (10).

Note that the operator L_n' is not self-adjoint. Therefore, the residual updating technique can be used in combination with an iterative solver for a non-self-adjoint problem such as BiCGSTAB method; see, e.g., [16]. The algorithm for the BiCGSTAB method is provided in Algorithm 3.

Algorithm 3 Biconjugate Gradient stabilized (BiCGSTAB) method

-
1. Initialize $\mathbf{x}_{(0)}$,
 2. Set $\mathbf{r}_{(0)} = \mathbf{b} - A\mathbf{x}_{(0)}$,
 3. Choose an arbitrary vector $\hat{\mathbf{r}}_{(0)}$ such that $(\hat{\mathbf{r}}_{(0)}, \mathbf{r}_{(0)}) \neq 0$, e.g., $\hat{\mathbf{r}}_{(0)} = \mathbf{r}_{(0)}$,
 4. Set $\rho_{(0)} = \alpha = \omega_{(0)} = 1$,
 5. Set $\mathbf{v}_{(0)} = \mathbf{p}_{(0)} = \mathbf{0}$,
 6. For $i = 1, 2, \dots$,
 - a. if $\|\mathbf{r}_{(i-1)}\| < \varepsilon$ stop,
 - b. $\rho_{(i)} = (\hat{\mathbf{r}}_{(0)}, \mathbf{r}_{(i-1)})$,
 - c. $\beta_{(i)} = (\rho_{(i)}/\rho_{(i-1)})(\alpha_{(i)}/\omega_{(i-1)})$,
 - d. $\mathbf{p}_{(i)} = \mathbf{r}_{(i-1)} + \beta_{(i)}(\mathbf{p}_{(i-1)} - \omega_{(i-1)}\mathbf{v}_{(i-1)})$,
 - e. $\mathbf{v}_{(i)} = A\mathbf{p}_{(i)}$,
 - f. $\alpha_{(i)} = \rho_{(i)}/(\hat{\mathbf{r}}_{(0)}, \mathbf{v}_{(i)})$,
 - g. $\mathbf{s}_{(i)} = \mathbf{r}_{(i-1)} - \alpha_{(i)}\mathbf{v}_{(i)}$,
 - h. $\mathbf{t}_{(i)} = A\mathbf{s}_{(i)}$,
 - i. $\omega_{(i)} = (\mathbf{t}_{(i)}, \mathbf{s}_{(i)})/(\mathbf{t}_{(i)}, \mathbf{t}_{(i)})$
 - j. $\mathbf{x}_{(i)} = \mathbf{x}_{(i-1)} + \alpha_{(i)}\mathbf{p}_{(i)} + \omega_{(i)}\mathbf{s}_{(i)}$,
 - k. $\mathbf{r}_{(i)} = \mathbf{s}_{(i)} - \omega_{(i)}\mathbf{t}_{(i)}$.
-

Algorithm 4 Residual updating algorithm - linear case

-
1. Initialize $\mathbf{g}_{(0)}^n$.
 2. Solve Stokes/Biot problem defined by (2) and (3) for $\mathbf{u}_f^n, p_f^n, \mathbf{u}_p^n, p_p^n, \boldsymbol{\eta}^n$.
 3. Compute $L(\mathbf{g}_{(0)}^n)$.
 4. Find the correction \mathbf{h}^n using the BiCGSTAB algorithm (Algorithm 3) with $A = L'_n(\mathbf{g}_{(0)}^n)$, $\mathbf{b} = -L_n(\mathbf{g}_{(0)}^n)$, and $\mathbf{x} = \mathbf{h}^n$.
 5. $\mathbf{g}^n \leftarrow \mathbf{g}_{(0)}^n + \mathbf{h}^n$.
-

5 Numerical Experiments

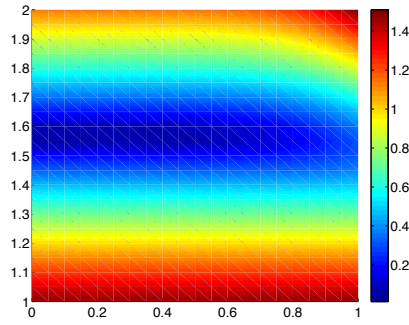
In order to investigate the convergence properties of Algorithms 2 and 4, we performed numerical experiments using a non-physical example.

We take $\Omega_p = (0, 1) \times (0, 1)$ for the poroelastic structure. The fluid domain $\Omega_f = (0, 1) \times (1, 2)$ is superposed on Ω_p , with the fluid-structure interface $\Gamma_I = \{(x, y) : 0 < x < 1, y = 1\}$. Also, the physical parameters are chosen as follows: $\nu_f = \nu_s = 0.5$, $\rho_f = \rho_s = 1$, $\alpha = \beta = \lambda = s_0 = \kappa = 1$. The right-hand side functions \mathbf{f}_f , \mathbf{f}_s , and f_p are chosen so that the exact solution is:

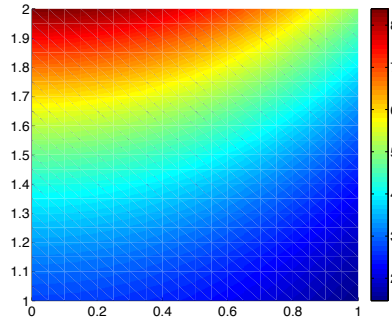
$$\begin{aligned}\mathbf{u}_f &= [(y-1)^2 x^3 (1+t^2), -\cos(y)e(1+t^2)], \\ p_f &= (\cos(x)e^y + y^2 - 2y + 1)(1+t^2), \\ \mathbf{u}_p &= [-x(\sin(y)e + 2(y-1))(1+t^2), (-\cos(y)e + (y-1)^2)(1+t^2)], \\ p_p &= (-\sin(y)e + \cos(x)e^y + y^2 - 2y + 1)(1+t^2), \\ \boldsymbol{\eta} &= [\sqrt{2} \cos(\sqrt{2}x) \cos(y)(1+t^2), \sin(\sqrt{2}x) \sin(y)(1+t^2)].\end{aligned}$$

The boundary and initial conditions are determined using the exact solution.

Figure 2 shows the magnitude of the fluid velocity and the fluid pressure at time $t = 0.0005$, while Figure 3 displays the magnitude of the structure displacement, the magnitude of the Darcy velocity, and the structure pressure at the same time.



(a) magnitude of \mathbf{u}_f



(b) pressure p_f

Fig. 2 Exact solution for the fluid problem at time $t = 0.0005$: (a) the magnitude of the fluid velocity and (b) the fluid pressure.

Note that the chosen exact solution does not satisfy all the interface conditions. Instead, it satisfies only (5b) and (5c), but not (5a) and (5d). Indeed, the exact

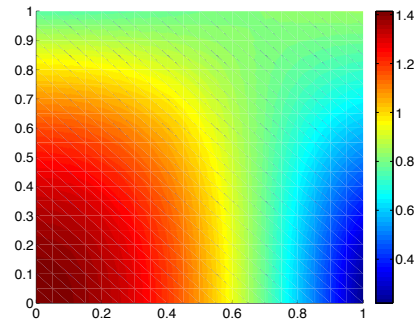
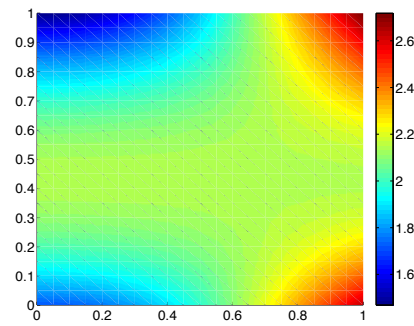
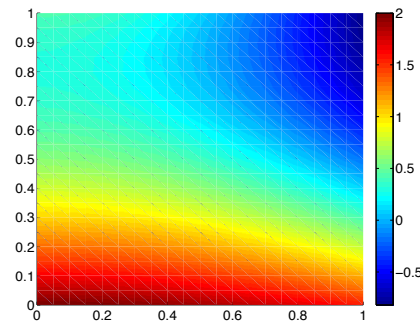
(a) magnitude of η (b) magnitude of \mathbf{u}_p (c) pressure p_p

Fig. 3 Exact solution for the structure problem at time $t = 0.0005$: (a) the magnitude of the structure displacement, (b) the magnitude of the Darcy velocity, and (c) the fluid pressure.

solution satisfies the following variations of (5a) and (5d):

$$\mathbf{u}_f \cdot \mathbf{n}_f = -\mathbf{u}_p \cdot \mathbf{n}_p, \quad (1a)$$

$$\mathbf{n}_f \cdot \boldsymbol{\sigma}_f \mathbf{t} = -\beta(\mathbf{u}_f \cdot \mathbf{t}). \quad (1b)$$

For our numerical implementation, we still implemented our algorithms as if all the interface conditions, (5a)–(5d), are satisfied. Then, to compensate the inexact interface conditions, we modified the functionals $N_n(\mathbf{g}^n)$ and $L_n(\mathbf{g}^n)$. More specifically, we compute the functional (5) with the additional term $-\eta_t \cdot \mathbf{n}$ for the first k entries and $+\beta \eta_t \cdot \mathbf{t}$ for entry $k+1$, where η_t is given by the chosen exact solution. Similarly, $-\eta_t \cdot \mathbf{n}$ and $+\beta \eta_t \cdot \mathbf{t}$ are added in the first and second entries of (17), respectively.

For the finite element approximations, we used inf-sup stable Taylor-Hood elements $\mathbb{P}_2 - \mathbb{P}_1$ on structured meshes for both (\mathbf{u}_f, p_f) and (\mathbf{u}_p, p_p) , and \mathbb{P}_2 elements for η . Because these elements are not stable for the Biot model, we added a stabilization term $\gamma(\nabla \cdot \mathbf{u}_p, \nabla \cdot \mathbf{v}_p)$ to the Darcy equation (3b) with $\gamma = 10$ and analogous terms were added to (10b) and (14b).

In order to verify the convergence of Algorithms 2 and 4, numerical experiments were performed with varying mesh sizes. The time step size Δt was set to 0.0001. The error tolerance for both CG and BiCGSTAB methods used in Algorithm 2 and Algorithm 4, respectively, was set to $\varepsilon = 10^{-5}$. We started with $\mathbf{g}_{(0)}^1 = -(0.1, 0.1)^T$ and $\mathbf{h}_{(0)}^1 = (0.01, 0.01)^T$ for the first time step. After the first time step, the initial stress function was chosen as $\mathbf{g}_{(0)}^n = \mathbf{g}^{n-1}$ for both algorithms.

First, we investigated Algorithm 2 through a mesh refinement study; we halved the mesh size in each mesh refinement. Table 1 reports the errors of finite element solutions with four different meshes at the fifth time step ($t = 0.0005$), where $(\mathbf{u}_f^h, p_f^h, \mathbf{u}_p^h, p_p^h, \eta^h)$, $(\mathbf{u}_f^{ex}, p_f^{ex}, \mathbf{u}_p^{ex}, p_p^{ex}, \eta^{ex})$ denote the finite element solution and the exact solution, respectively. The rates of convergence of all the quantities in the respective norms are those predicted by the theory.

h	$\ \mathbf{u}_f^h - \mathbf{u}_f^{ex}\ _{0,\Omega^f}$	rate	$ \mathbf{u}_f^h - \mathbf{u}_f^{ex} _{1,\Omega^f}$	rate	$\ p_f^h - p_f^{ex}\ _{0,\Omega^f}$	rate
1/2	1.18×10^{-2}	–	1.59×10^{-1}	–	1.38×10^{-1}	–
1/4	1.26×10^{-3}	3.23	3.59×10^{-2}	2.15	2.51×10^{-2}	2.46
1/8	1.43×10^{-4}	3.14	8.69×10^{-3}	2.05	5.25×10^{-3}	2.26
1/16	1.75×10^{-5}	3.03	2.15×10^{-3}	2.02	1.21×10^{-3}	2.12
h	$ \mathbf{u}_p^h - \mathbf{u}_p^{ex} _{H^{div}(\Omega^p)}$	rate	$\ p_p^h - p_p^{ex}\ _{0,\Omega^p}$	rate	$ \eta^h - \eta^{ex} _{1,\Omega^p}$	rate
1/2	7.12×10^{-3}	–	4.58×10^{-2}	–	6.33×10^{-2}	–
1/4	1.93×10^{-3}	1.88	1.12×10^{-2}	2.03	1.58×10^{-2}	2.00
1/8	4.72×10^{-4}	2.03	2.78×10^{-3}	2.01	3.95×10^{-3}	2.00
1/16	1.16×10^{-4}	2.02	6.95×10^{-4}	2.00	9.87×10^{-4}	2.00

Table 1 Errors and convergence rates using Algorithm 2 at the fifth time step ($t = 0.0005$) with $\Delta t = 0.0001$.

Table 2 and 3 report the number of CG iterations for Algorithm 2 together with the initial and final values of the objective functional \mathcal{J}_n defined in (4) at the first time step and at the fifth time step, respectively. We remark that while at the first time step the number of CG iterations more than doubles every time the mesh size is halved, it is no more the case at the fifth time step when going from the third to the fourth mesh refinement. Recall that we make a random initial choice for $\mathbf{g}_{(0)}^1$. At every successive step, however, we set $\mathbf{g}_{(0)}^n = \mathbf{g}^{n-1}$. Therefore, the initial value of \mathcal{J}_n is much larger at the first time step than at the fifth. Note that the initial value of \mathcal{J}_n at the fifth time step is already around 10^{-5} .

h	No. of CG iter.	Initial \mathcal{J}_n	Terminal \mathcal{J}_n
1/2	10	1.12×10^3	6.63×10^{-8}
1/4	26	7.54×10^2	8.49×10^{-7}
1/8	62	2.44×10^2	2.91×10^{-7}
1/16	161	7.25×10^1	9.49×10^{-8}

Table 2 Number of CG iterations for Algorithm 2, initial and terminal functional values at the first time step ($t = 0.0001$) with $\Delta t = 0.0001$.

h	No. of CG iter.	Initial \mathcal{J}_n	Terminal \mathcal{J}_n
1/2	9	2.58×10^{-5}	1.30×10^{-14}
1/4	21	3.64×10^{-5}	1.23×10^{-12}
1/8	57	5.16×10^{-6}	3.31×10^{-14}
1/16	94	2.85×10^{-7}	1.92×10^{-12}

Table 3 Number of CG iterations for Algorithm 2, initial and terminal residual values for the fifth time step ($t = 0.0005$) with $\Delta t = 0.0001$.

Next, we investigated Algorithm 4. We observed that Algorithm 4 gave almost identical errors to the ones reported in Table 1, hence the report is omitted here. The number of BiCGSTAB iterations for Algorithm 4, and the initial and final values of \mathcal{J}_n at the first time step and at the fifth time step are presented in Tables 4 and 5, respectively.

We observe that at the first time step, with an arbitrarily chosen $\mathbf{g}_{(0)}^1$, the number of CG iterations needed is similar to or a little more than that of BiCGSTAB iterations. However, at the fifth time step, where the iterations start with a more accurate initial control $\mathbf{g}_{(0)}^5 = \mathbf{g}^4$, significantly less iterations are needed for CG than BiCGSTAB iterations. This gets more prominent as h gets smaller.

As far as computational effort is concerned, the computational cost per iteration is almost the same for both algorithms. More specifically, in each CG iteration, (9)–(10), and (13)–(14) need to be solved, while in each BiCGSTAB iteration, (9)–(10) need to be solved twice with different right-hand sides.

h	No. of BiCGSTAB iter.	Initial \mathcal{J}_n	Terminal \mathcal{J}_n
1/2	8	1.34×10^3	1.05×10^{-7}
1/4	23	8.69×10^2	1.16×10^{-6}
1/8	68	2.64×10^2	7.17×10^{-7}
1/16	132	7.52×10^1	6.77×10^{-7}

Table 4 Number of BiCGSTAB iterations for Algorithm 4, initial and terminal functional values at the first time step ($t = 0.0001$) with $\Delta t = 0.0001$.

h	No. of BiCGSTAB iter.	Initial \mathcal{J}_n	Terminal \mathcal{J}_n
1/2	7	1.20×10^{-3}	3.91×10^{-11}
1/4	34	1.70×10^{-4}	2.69×10^{-11}
1/8	121	1.34×10^{-5}	2.43×10^{-11}
1/16	263	4.94×10^{-7}	3.85×10^{-11}

Table 5 Number of BiCGSTAB iterations for Algorithm 4, initial and terminal residual values for the fifth time step ($t = 0.0005$) with $\Delta t = 0.0001$.

6 Conclusions

We have studied the interaction of a free-fluid with a poroelastic structure, modeled by the Stokes-Biot system. After discussing the time-discretized variational formulation of the coupled problem, we developed a minimization problem in which the Stokes-Biot system was decoupled through a control function on the interface. Two numerical algorithms based on a residual updating technique have been proposed; one solves a least squares problem and the other solves a linear problem when the solution \mathbf{u}_p is smooth enough. We observed that both algorithms yielded an optimal control function along with a solution for the Stokes-Biot system that satisfies the interface conditions. Also, the optimal rates of convergence for finite element solutions demonstrate that there was no spatial degradation of the solution over time steps. On the other hand, the proposed decoupling schemes enable us to solve the two subproblems in parallel and they can be easily extended to a nonlinear system,

e.g., the coupled Navier-Stokes and Biot system. Subsequent work will provide an analytical framework for the proposed methods and include numerical experiments that are designed for moving domains in a physical setting.

Acknowledgements This work was supported by the Institute for Mathematics and its Applications (IMA), which is funded by the National Science Foundation (NSF). A. Cesmelioglu would like to thank Oakland University for the URC Faculty Research Fellowship Award. H. Lee was supported by NSF under contract number DMS 1418960 and A. Quaini's research was supported in part by NSF under grant DMS-1262385. The research of S.-Y. Yi was supported by NSF under contract number DMS 1217123.

References

1. M. A. Murad, J. N. Guerreiro, and A. F. D. Loula. Micromechanical computational modeling of reservoir compaction and surface subsidence. *Math. Contemp.*, 19:41–69, 2000.
2. M. A. Murad, J. N. Guerreiro, and A. F. D. Loula. Micromechanical computational modeling of secondary consolidation and hereditary creep in soils. *Comput. Methods Appl. Mech. Engrg.*, 190(15-17):1985–2016, 2001.
3. N. Koshiba, J. Ando, X. Chen, and T. Hisada. Multiphysics simulation of blood flow and LDL transport in a porohyperelastic arterial wall model. *J. of Biomech. Eng.*, 129:374–385, 2007.
4. V. M. Calo, N. F. Brasher, Y. Bazilevs, and T. J. R. Hughes. Multiphysics model for blood flow and drug transport with application to patient-specific coronary artery flow. *Comput. Mech.*, 43(1):161–177, 2008.
5. S. Badia, A. Quaini, A. Quateroni, Coupling Biot and Navier-Stokes equations for modeling fluid-poroelastic media interaction, *Journal of Computational Physics*, 228 (2009) 7986–8014.
6. B. Tully and Y. Ventikos. Coupling poroelasticity and CFD for cerebrospinal fluid hydrodynamics. *Biomedical Engineering, IEEE Transactions on*, 56(6):1644–1651, 2009.
7. B. Ganis, R. Liu, B. Wang, M.F. Wheeler, and I. Yotov. Multiscale modeling of flow and geomechanics. *Radon Series on Computational and Applied Mathematics*, pages 165–204, 2013.
8. M. Bukac, I. Yotov, and P. Zunino, An operator splitting approach for the interaction between a fluid and a multilayered poroelastic structure. *Numerical Methods for Partial Differential Equations*, 31(4): 1054–1100, 2015.
9. M. Bukač, I. Yotov, R. Zakerzadeh and P. Zunino, Partitioning strategies for the interaction of a fluid with a poroelastic material based on a Nitsches coupling approach, *Computer Methods in Applied Mechanics and Engineering*, 292: 138–170, 1 August 2015.
10. M. A. Biot. General theory of three-dimensional consolidation. *J. Appl. Phys.*, 12:155–164, 1941.
11. M. A. Biot. Theory of elasticity and consolidation for a porous anisotropic solid. *J. Appl. Phys.*, 25:182–185, 1955.
12. M. A. Biot. Theory of finite deformations of porous solids. *Indiana Univ. Math. J.*, 21:597–620, 1972.
13. O. Coussy. *Mechanics of Porous Continua*. John Wiley & Sons, 1995.
14. R. E. Showalter. Poroelastic filtration coupled to Stokes flow. In O. Imanuvilov, G. Leugering, R. Triggiani, and B. Zhang, editors, *Lecture Notes in Pure and Applied Mathematics*, vol. 242, pages 229–241. Chapman & Hall, Boca Raton, 2005.
15. V.J. Ervin, E.W. Jenkins, and H. Lee. Approximation of the Stokes-Darcy system by optimization, *J. Sci. Comput.*, 59 (2014) 775–794.

16. Y. Saad, *Iterative Methods for Sparse Linear Systems*, Second Edition, SIAM, Philadelphia, PA, 2003. MR1990645.
17. P. Kuberry and H. Lee. A decoupling algorithm for fluid-structure interaction problems based on optimization. *Comput. Methods. Appl. Mech. Engrg.*, 267: 594–605, 2013